Computational Mathematics and Mathematical Physics, Vol. 45, No. 4, 2005, pp. 666–676.
Translated from Zhurnal Vychislitel'noi Matematiki i Matematicheskoi Fiziki, Vol. 45, No. 4, 2005, pp. 690–700.

Modeling of Volume Free Electron Lasers

K. G. Batrakov and S. N. Sytova

Institute for Nuclear Problems, Belarussian State University, Bobruiskaya ul. 11, Minsk, 220050 Belarus
e-mail: batrakov@inp.minsk.by, sytova@inp.minsk.by

Received July 19, 2004

Abstract—Numerical methods for solving systems of differential equations arising in the simulation of volume free electron lasers are developed, and numerical experiments are discussed.

Keywords: modeling of volume lasers, numerical algorithm.

1. INTRODUCTION

The conversion of the kinetic energy of an electron beam into radiation energy underlies the operation of many electronic devices. They include traveling wave tubes (TWT), backward wave tubes (BWT), and free electron lasers (FEL). The electromagnetic generators and amplifiers available at present cover wavelengths from the microwave to the ultraviolet vacuum range [1–4]. FEL lasing in the ultraviolet range has been obtained relatively recently on the basis of self-amplified stimulated emission (SASE). Despite the success achieved in this area, there are many problems to be solved. One of them is that the generation frequency cannot be tuned in a wide spectral range. As a rule, high-efficiency lasers have optimal preliminarily designed parameters (such as electron beam characteristics, the waveguide and resonator sizes, the undulator and grating periods, modulation, etc.). Variations in any of these parameters as required for frequency tuning sharply reduce the efficiency of lasing. Another difficulty arises in high power lasing. In the generation of pulses with power higher than 10 GW, it is highly desirable that the cross section of the electron beam be large in order to reduce the current density occurring at a high total current. However, when the linear sizes of the cross section exceed the generated wavelength, a large number of parasitic modes are excited in the resonator (waveguide), which leads to destructive interference and, as a consequence, to a sharp fall in the efficiency of the generation.

A possible way of overcoming the above difficulties is to use volume distributed feedback (VDFB) in volume free electron lasers (VFEL). The principles and theoretical foundations of VFEL operation were laid in [5, 6]. A major advantage of VFEL is that it provides mode discrimination in an oversized system. The volume nature of VDFB makes it possible to vary the VDFB geometry or the electron beam position relative to the structure and to vary the generated wave frequency. VFEL lasing in the millimeter range was first obtained experimentally at the Institute for Nuclear Problems of Belarussian State University [7].

The linear stage in VFEL operation has been fairly thoroughly investigated to this day. The threshold generation currents, spectral-angular distributions, and the times of VFEL instability development were found for various radiation mechanisms (parametric, undulator, Smith–Purcell) [7–21]. In VFEL operation, the linear stage quickly gives way to the nonlinear stage, at which most of the electron beam energy is transformed into radiation. For this reason, a detailed analysis is required for the nonlinear stage of VFEL, the regimes of generation, amplification, and regenerative amplification at the nonlinear saturation stage, and for the influence exerted on these regimes by gradual variations in the VDFB geometry. Computations of this kind are necessary for experiment design, optimal geometry determination, and result processing.

An analytical analysis can be performed only for the linear stage and some partial features of the nonlinear stage, because mathematical models describing the nonlinear stage of VFEL operation are very complicated. They are given by systems of multidimensional nonlinear integro-differential and partial differential equations. The boundary conditions specified on the various boundaries of the system can include first-order partial differential equations unsolved for the time derivatives of several unknown functions. For this reason, a detailed numerical analysis is required for describing the nonlinear stage of VFEL operation. Problems of this kind can arise in other areas of physics (e.g., in hydrodynamics, radiation transfer theory), chemistry, etc. The aforesaid testifies to the importance of this study.

Numerous papers are available that deal with FEL simulation (see [22–25]). Mathematical models of various VFEL types in the X-ray, optical, and millimeter wave ranges were considered in [26–36]. Earlier, an electron beam was simulated in the hydrodynamic approximation [26, 27] or the kinetic approximation

with the use of distribution functions [28–30]. These methods perform well when the electron beam current density is low but give rise to instability as its magnitude increases, which is explained by possible intersections of different electron beam trajectories at large current and electromagnetic field values. Following [36], we model the electron beam by means of the phase averaging method, which has been used earlier in TWT, BWT, and FEL simulation.

2. PHYSICAL MODEL OF VFEL

The electron beam in VFEL can pass near a three-dimensional periodic structure [14, 15] or through it [9–11, 18]. In the general case, the Bragg VDFB in VFEL is formed by n strongly coupled waves (the so-called n-wave Bragg diffraction). In the special case of two-wave diffraction, two fundamentally different geometries are possible: Bragg geometry with oppositely directed waves and Laue geometry with waves propagating in the same direction. Figure 1 shows a three-dimensional VFEL scheme in Bragg geometry. The electron beam with velocity $\mathbf{u}$ is incident at some angle on a spatially periodic target of thickness L. Simultaneously, an electromagnetic wave (*1*) with the frequency ω and the wave vector $\mathbf{k}$ is incident on the system. If the diffraction conditions are satisfied [37], then a strong diffracted wave (*2*) with the wave vector $\mathbf{k}_\tau = \mathbf{k} + \tau$, where τ is the reciprocal lattice vector, arises in the target. For the beam of electrons to group into a radiating phase and to generate radiation, it is necessary that the phase velocity of the electromagnetic wave be somewhat lower than the velocity of the electron beam. The equality between these velocities is expressed by the well-known Vavilov–Cherenkov condition

$$\omega - \mathbf{ku} = 0. \tag{1}$$

The typical value of the deviation from (1) is determined by the length of the domain where the electron beam interacts with the wave (in the case of a weak gain) or by the electron beam density (in the case of a high gain [10]). Electron beam instability arises under the synchronism conditions and results in the generation of quasi-Cherenkov radiation. Crystalline plates are used as a target in the x-ray region. In this case, the spatial period is determined by the crystal lattice period and the radiation generated has a length comparable with interatomic distances, i.e., belongs to the X-ray region. An artificial grating or a corrugated waveguide can be used as a target in the microwave region. A volume periodic system consisting of periodically arranged dielectric or metallic filaments was considered in [18].

In Laue geometry, the incident and diffracted waves propagate in the same direction (Fig. 2a). In both geometries, two waves (waves *1* and *3*) with a given amplitude can be incident on the system (in the case of amplifier simulation). In Bragg geometry, the generator regime is also considered at which there are no waves incident on the system. We also simulated the case of VFEL with external mirrors, which is schematically shown in Fig. 1b. Generally, two waves are simultaneously incident on a periodic lattice.

Several operation regimes can be realized in Bragg geometry: (i) the current is lower than a critical value and no radiation is generated; (ii) when the critical current is reached, a regime is possible at which the incident electromagnetic waves are amplified by the electron beam (the so-called regime of regenerative ampli-

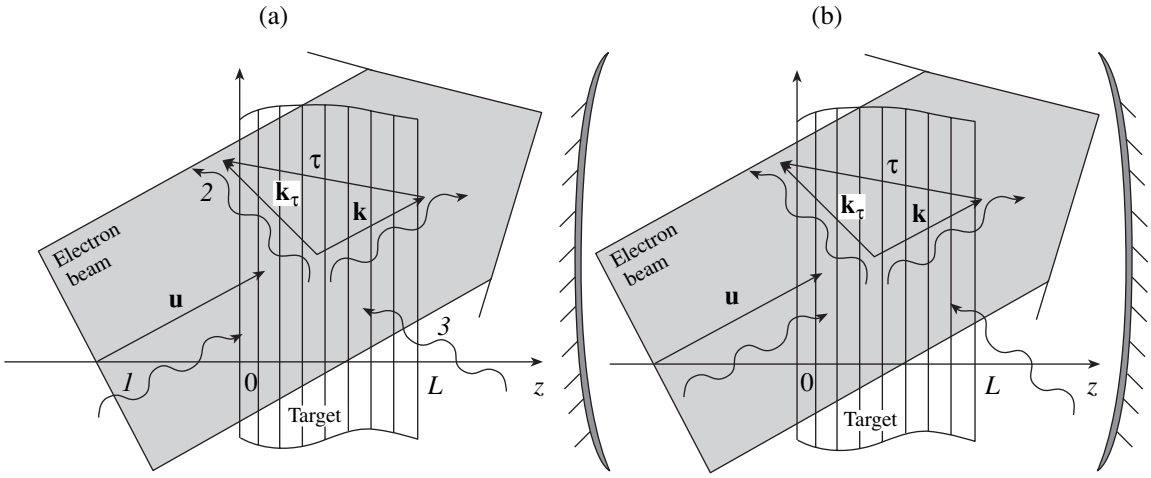

Fig. 1.

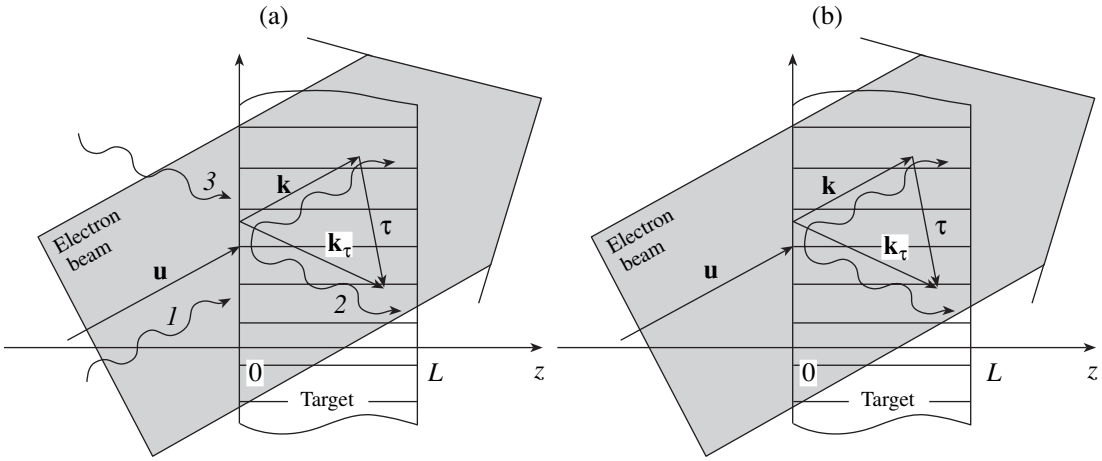

Fig. 2.

fication); and (iii) as the current further increases and exceeds a threshold (j_{thresh}), the generation regime is established.

In Laue geometry, radiation can be generated even in the absence of an incident wave (Fig. 2b), which is the so-called SASE regime [38]. The SASE regime in Laue geometry and the generation regime in Bragg geometry develop from spontaneous noises. The generation regime in a system with Laue geometry becomes possible after external mirrors are added to the system [17].

In this paper, the nonlinear stage of the VFEL regimes listed above is analyzed by methods of mathematical modeling.

3. MATHEMATICAL MODEL OF VFEL

The equations describing VFEL operation are deduced from Maxwell equations in the approximation of slowly varying amplitudes. The first two Maxwell equations yield the single second-order equation

$$\Delta\mathbf{E} - \nabla(\nabla\mathbf{E}) - \frac{1}{c^2}\frac{\partial^2\mathbf{E}}{\partial t^2} = \frac{\partial\mathbf{j}_b}{\partial t}, \tag{2}$$

where $\mathbf{E}$ is the electric field strength and $\mathbf{j}_b$ is the current density of the electron beam.

In the case of two-wave diffraction, these quantities are substituted into (2) in the form

$$\mathbf{E} = \mathbf{e}_\sigma(Ee^{i(\mathbf{kr}-\omega t)} + E_\tau e^{i(\mathbf{k}_\tau\mathbf{r}-\omega t)}),$$

$$\boldsymbol{j}_b = \mathbf{e}_\sigma j e^{i(\mathbf{kr}-\omega t)},$$

where i is the imaginary unit and $\mathbf{e}_\sigma$ is the sigma polarization vector [37].

In the approximation of slowly varying amplitudes, i.e., in the case where

$$\left|\frac{1}{k}\frac{\partial E}{\partial\mathbf{r}}\right| \ll |E|, \quad \left|\frac{1}{\omega}\frac{\partial E}{\partial t}\right| \ll |E|, \quad k = \omega/c,$$

the second derivatives with respect to time and space can be neglected.

The electron beam equations can be obtained in the hydrodynamic approximation, by means of distribution functions, or with the help of the phase averaging method. In [28–30], the dynamics of an electron beam were simulated with the help of a kinetic equation and distribution functions in the optical range for the surface VFEL scheme. In this paper, electron beam dynamics in VFEL is modeled by averaging over the initial electron phases when they enter the interaction region [35]. This method is well known and is widely applied to the calculation of TWT, BWT, FEL, and other electronic devices.

Let us derive an expression for the electron beam current. The incident magnetic field is assumed to be such that the beam is magnetized. Electron beam dynamics is one-dimensional. The equation of motion of

a single electron moving in the wave field is given by

$$\ddot{z} = \frac{e}{m\gamma^3}(\mathbf{e}_\sigma \mathbf{n})\mathrm{Re}\{a\exp(i\mathbf{k}_\perp \mathbf{r}_\perp + ik_z z - i\omega t)\},$$

where γ is the Lorentz factor of the electron beam, $\mathbf{n}$ is the normal vector to the target surface, and k_z is the projection of the wave vector $\mathbf{k}$ on the z axis. It is not possible to trace the motion of a single electron in the beam. Every electron can be characterized by its initial phase when entering the domain of interaction. This initial phase is an individual characteristic of each electron in the beam. Averaging over this phase on the wavelength makes it possible to proceed from the microscopic to macroscopic description. The current thus averaged is given by

$$j = \frac{en_0 u}{2\pi}\frac{1}{2\pi}\int_0^{2\pi} d\Theta_1 \int_{\omega(t-z/u)}^{\omega(t-z/u)+2\pi} d\Theta_0 \exp[-i\Theta(t, \Theta_1 - \Theta_0)]. \tag{3}$$

Here, n_0 is the density of particles in the beam, u is their initial velocity, $\Theta(t, t_0, \mathbf{r}_\perp) = k_z z + \mathbf{k}_\perp \mathbf{r}_\perp - \omega t(z, t_0)$ is the electron phase in the wave, and $t(z, t_0)$ is the trajectory of an electron entering the interaction region at time t_0. The initial electron phase is given by

$$\Theta(t = t_0, t_0, \mathbf{r}_\perp) = \mathbf{k}_\perp \mathbf{r}_\perp - \omega t_0 = \Theta_1 - \Theta_0.$$

In contrast to the undulator system, in which the dynamics of an electron is determined only by the entrance time t_0, in our case, the electron dynamics is also affected by the spatial cross point of beam entrance in the interaction region Θ_1. Thus, the transition to a macroscopic description is associated with averaging over two phases. Averaging makes use of the Liouville theorem. In this case, the Liouville theorem is equivalent to the particle conservation law and is reduced to the following equality in the one-dimensional case:

$$jdt = j_0 dt_0.$$

This equality is very useful for averaging the current on the wave oscillation period. By simple rearrangement, averaging over the phases Θ_0 and Θ_1 in (6) is reduced to averaging over a single phase $p \in [-2\pi, 2\pi]$.

Thus, the general mathematical model of a VFEL (Fig. 1) is given by

$$\frac{\partial E}{\partial t} + a_1\frac{\partial E}{\partial z} + b_{11}E + b_{12}E_\tau = \Phi j, \quad \frac{\partial E_\tau}{\partial t} + a_2\frac{\partial E_\tau}{\partial z} + b_{21}E + b_{22}E_\tau = 0, \tag{4a}$$

$$j = \int_0^{2\pi} \frac{2\pi - p}{8\pi^2}\{\exp[-i\Theta(t, z, p) + \exp(-i\Theta(t, z, -p)]\}dp, \tag{4b}$$

$$\frac{d^2\Theta(t, z, p)}{dz^2} = \Psi\left(k - \frac{d\Theta(t, z, p)}{dz}\right)^3 \mathrm{Re}\{E(t - z/u, z)\exp[i\Theta(t, z, p)]\}, \tag{4c}$$

$$E|_{t=0} = 0, \quad E_\tau|_{t=0} = 0, \tag{4d}$$

$$E|_{z=0} = E_0, \quad E_\tau|_{z=L} = E_{\tau 0}, \tag{4e}$$

$$\Theta(t, 0, p) = p, \quad \frac{d\Theta(t, 0, p)}{dz} = k_z - \omega/u, \quad t > 0, \quad z \in [0, L], \quad p \in [-2\pi, 2\pi], \tag{4f}$$

where E_0 and $E_{\tau 0}$ are the amplitudes of the waves incident on the target. In addition to time, the spatial coordinate z and the electron initial phase p are considered in system (4). The electromagnetic field amplitudes $E(t, z)$ and $E_\tau(t, z)$ and the coefficients a, b, and Φ are complex-valued. The function $\Theta(t, z, p)$ describes the phase of the electron beam relative to the electromagnetic wave. The function Θ and the coefficients Ψ are real-valued.

At the initial stage of the laser operation, a linear nonstationary process develops that is characterized by exponentially increasing fields. As the electron kinetic energy is conversed into electromagnetic wave energy, the velocity of the electrons reduces and the synchronism conditions are violated for them. This process occurs at the nonlinear stage. Moreover, the system passes into a steady-state regime. The system

describing the steady-state regime of VFEL operation takes the form

$$\frac{dE}{dz} + a_{11}E + a_{12}E_\tau = \Phi j, \quad \frac{dE_\tau}{dz} + a_{21}E + a_{22}E_\tau = 0, \tag{5a}$$

$$\frac{d^2\Theta(z,p)}{dz^2} = \Psi\left(k - \frac{d\Theta(z,p)}{dz}\right)^3 \mathrm{Re}[E(z)\exp(i\Theta(z,p))]. \tag{5b}$$

Boundary conditions (4e) and (4f) and the formula for the beam current density (4b) remain unchanged.

Boundary conditions (4e) are written out for the Bragg case (Fig. 1). In Laue geometry (Fig. 2), they are given by

$$E|_{z=0} = E_0, \quad E_\tau|_{z=0} = E_{\tau 0}. \tag{6}$$

In the presence of external mirrors, boundary conditions (4e) are generalized as follows:

$$E|_{z=0} = E_0 + \alpha_1 E|_{z=L}\exp(i\varphi_1) + \alpha_2 E_\tau|_{z=0}\exp(i\varphi_2),$$

$$E_\tau|_{z=L} = E_{\tau 0} + \alpha_3 E|_{z=L}\exp(i\varphi_3) + \alpha_4 E_\tau|_{z=0}\exp(i\varphi_4).$$

Here, α_i and φ_i are the amplitudes and phases of the coupling coefficients of the corresponding waves in reflection.

In the case of external mirrors, the boundary conditions in Laue geometry (6) are specified as

$$\begin{aligned} E|_{z=0} &= E_0 + \alpha_1 E|_{z=L}\exp(i\varphi_1) + \alpha_2 E_\tau|_{z=L}\exp(i\varphi_2), \\ E_\tau|_{z=0} &= E_{\tau 0} + \alpha_3 E|_{z=L}\exp(i\varphi_3) + \alpha_4 E_\tau|_{z=L}\exp(i\varphi_4). \end{aligned} \tag{7}$$

It is assumed that all the functions are smooth, bounded, and slowly varying.

4. FINITE DIFFERENCE METHODS

In what follows, wherever convenient, we use the notation adopted in [39].

First, we consider a finite-difference scheme for system (4). In the domain

$$\Omega \cap \Omega_t = \{0 \le z \le L, -2\pi \le p \le 2\pi\} \cap \{t > 0\},$$

we introduce the uniform grids

$$\omega_t = \{t_l = lh_t, l = 0, 1, \ldots\}, \quad \omega_z = \{z_m = mh_z, m = 0, 1, \ldots, M, Mh_z = L\},$$

$$\omega_p = \{p_j = h_p j, j = -N, \ldots, -1, 0, 1, \ldots, N, h_p N = 2\pi\}.$$

Then, we can write down

$$\hat{\Theta}^j_{\bar{z}z} = \Psi(k - \hat{\Theta}^j_{\circ z})^3 \mathrm{Re}[\tilde{E}\exp(i\Theta^j)], \quad j = 0, \pm 1, \ldots, \pm N, \tag{8a}$$

$$E_t + a_1\hat{E}_{\bar{z}} + b_{11}\hat{E} + b_{12}\hat{E}_\tau = \Phi\sum_{j=0}^{N} c_j[\exp(-i\hat{\Theta}^j) + \exp(-i\hat{\Theta}^{-j})], \tag{8b}$$

$$E_{\tau t} + a_2\hat{E}_{\tau z} + b_{21}\hat{E} + b_{22}\hat{E}_\tau = 0, \tag{8c}$$

where

$$\tilde{E} = E(t_l - \eta t_m, z_m), \quad \eta = h_z/(h_t u)$$

and c_j are the coefficients of the quadrature formula. The integer part of η was used in the computations. When $t_l - \eta t_m < 0$, we set $\tilde{E} = E(0, z_m)$. The trapezoid rule was used for numerical integration.

For stationary system (5), we propose the iterative algorithm

$$\overset{s+1}{\Theta}{}^j_{\bar{z}z} = \Psi(k - \overset{s+1}{\Theta}{}^j_{\circ z})^3 \mathrm{Re}[\overset{s}{E}\exp(i\overset{s+1}{\Theta}{}^j)], \quad j = 0, \pm 1, \ldots, \pm N, \tag{9a}$$

$$\overset{s+1}{E}_{\bar{z}} + a_{11}\overset{s+1}{E} + a_{12}\overset{s+1}{E}_{\tau} = \Phi\sum_{j=0}^{N} c_j[\exp(-i\overset{s+1}{\Theta^j}) + \exp(-i\overset{s+1}{\Theta^{-j}})], \tag{9b}$$

$$\overset{s+1}{E}_{\tau z} + a_{21}\overset{s+1}{E} + a_{22}\overset{s+1}{E}_{\tau} = 0, \tag{9c}$$

where $s = 0, 1, \ldots$ is the iteration index. We set $\overset{0}{\Theta}^j = h_p j$, $\overset{0}{E} = 0$, and $\overset{0}{E}_{\tau} = 0$ at interior grid points.

Differential equation (9a) can be rewritten as

$$\frac{\overset{s+1}{\Theta}^j_{m+1} - 2\overset{s+1}{\Theta}^j_m + \overset{s+1}{\Theta}^j_{m-1}}{h_z^2} = \Psi\left(k - \frac{\overset{s+1}{\Theta}^j_{m+1} - \overset{s+1}{\Theta}^j_{m-1}}{2h_z}\right)^3 \mathrm{Re}[\overset{s}{E}\exp(i\overset{s+1}{\Theta}^j_m)].$$

This is an implicit cubical difference equation in the unknown $\overset{s+1}{\Theta}^j_{+1}$. When solving this equation, we choose the root that is close to the neighboring values. The other two roots make no sense. Equation (8a) is solved in a similar manner.

In all the cases, the boundary conditions can be written precisely.

Laue geometry differs from Bragg geometry by the propagation direction of the diffracted wave. All the schemes above were written for Bragg geometry (with the right discrete derivative with respect to z written for the wave E_i). In the Laue case, it should be replaced by the left discrete derivative.

Since finite-difference schemes (8) and (9) are strongly nonlinear, we cannot analyze their rate of convergence and convergence, while the convergence analysis of linearized schemes is trivial. For this reason, we only show how the solution attains a steady state in the iteration process (see Fig. 3). About 10 iterations are required in the domain where the generation threshold is overpassed and far away (curve *1*) or amplification is virtually absent (curve *2*). Usually, a steady-state solution is attained in several tens of iteration steps (curve *3*). Several hundred iteration steps can be required near the generation threshold, where a steady-state solution is attained slowly (curve *4*). The process of attaining a steady-state solution to the nonstationary system will be discussed below.

Let us discuss the question of where radiation in the system is generated from when there are no incident waves (the generator regime). In actual physical systems, radiation is produced and amplified from spontaneous noises. In numerical modeling, this is associated with computational errors in the integral on the right-hand side of the equations. Clearly, at the first iteration step or at the initial time, we have

$$I = \Phi\int_0^{2\pi}\frac{2\pi - p}{8\pi^2}\{\exp[-i\Theta(z, p)] + \exp[-i\Theta(z, -p)]\}dp \equiv 0$$

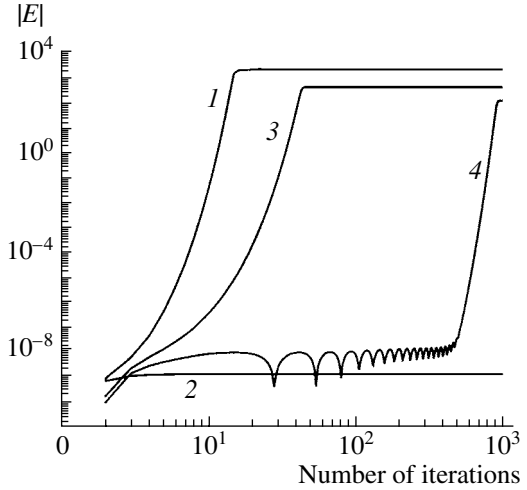

Fig. 3.

everywhere inside the domain $z \in [0, L]$. However, $I \sim 10^{-15}$ in reality. This is an equivalent of spontaneous noises and a trigger for the generation process.

5. NUMERICAL RESULTS FOR VFEL

Based on the finite-difference methods proposed, a software package has been developed for the numerical modeling of quasi-Cherenkov VFEL operation. We demonstrate a small number of examples of the successful package performance that characterize all the basic features in the behavior of electromagnetic fields for two-wave quasi-Cherenkov VFEL generating radiation in the millimeter wavelength range. The numerical results obtained agree entirely with the analytical estimates and the expected behavior of the solution.

It should be emphasized that we also modeled VFEL operation in the X-ray range. However, since many physical and engineering problems (such as multiple particles scattering in crystals, etc.) have not been solved in this range thus far, the creation of an X-ray quasi-Cherenkov VFEL for the electron beams available is not possible.

The starting currents of the electron beam, the radiation power, and the radiation frequency depend on the geometry of the VDFB. Changing this geometry, we can change these characteristics and switch from the generation regime to the amplification regime and vice versa. Altogether, there are more than ten initial parameters of the system that influence its qualitative behavior. Figures 4 and 5 show the numerical results for stationary system (5). The threshold current density is a very important characteristic describing the behavior of the system. Figure 4 displays the amplitude of the electromagnetic field as a function of the beam current density in Bragg geometry for an idealized system (a) without absorption (the imaginary part of the dielectric permittivity χ_0 is zero) and (b) with absorption. The main goal was to analyze the amplification regime in Bragg geometry ($L = 20$ cm). As expected, the generation threshold increases in the case of absorption or when it increases. In both plots, this threshold is shown by line B. The range between lines A and B corresponds to the regime of amplification. As absorption increases, the width of this range increases by one order of magnitude. The increase in the width of the amplification range is determined by the balance between the rate of radiation generation in the wave synchronous with the electron beam and the rate of radiation absorption of the diffracted wave, which provides distributed feedback in the generator. As absorption increases, the size of the domain where radiation absorption in the backward wave exceeds the radiation generation in the synchronous wave increases as well. The domain with such parameters corresponds to the regime of regenerative amplification. Figure 5a shows the generation threshold as a function of the target length (the solid curve corresponds to $E_0 = 0$ and $\chi_0 = 0.1$, and the dashed curve, to $\chi_0 = (0.1, 0.001)$. The plot displays the generation threshold with and without absorption in the target. The larger the thickness of the target, the lower the threshold. The functional dependence of the generation threshold on the length changes. Analytical estimates suggest that, for short lengths, the threshold current is inversely proportional to the fifth power of the target length. As the target length increases, this dependence becomes milder. In the ideal case, where the length is long and absorption is taken into account, the threshold current

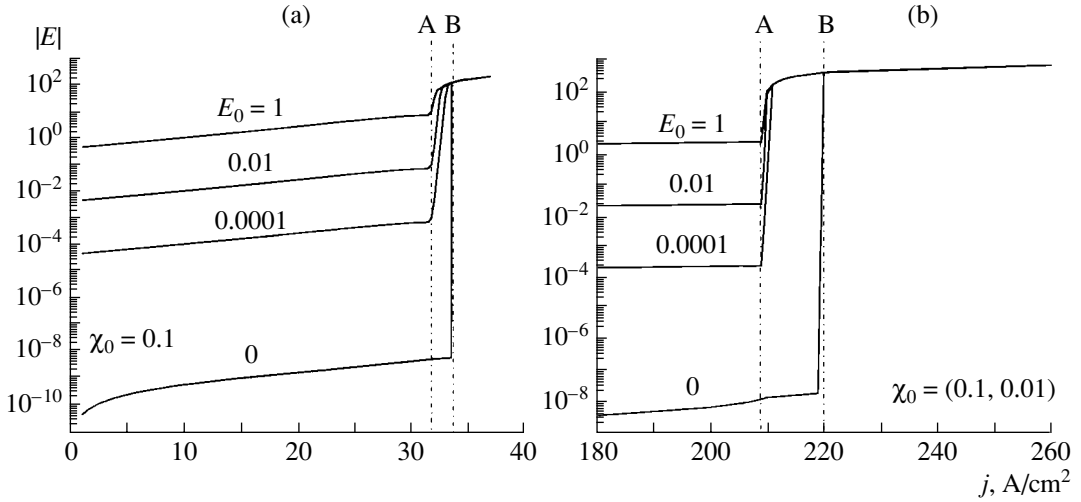

Fig. 4.

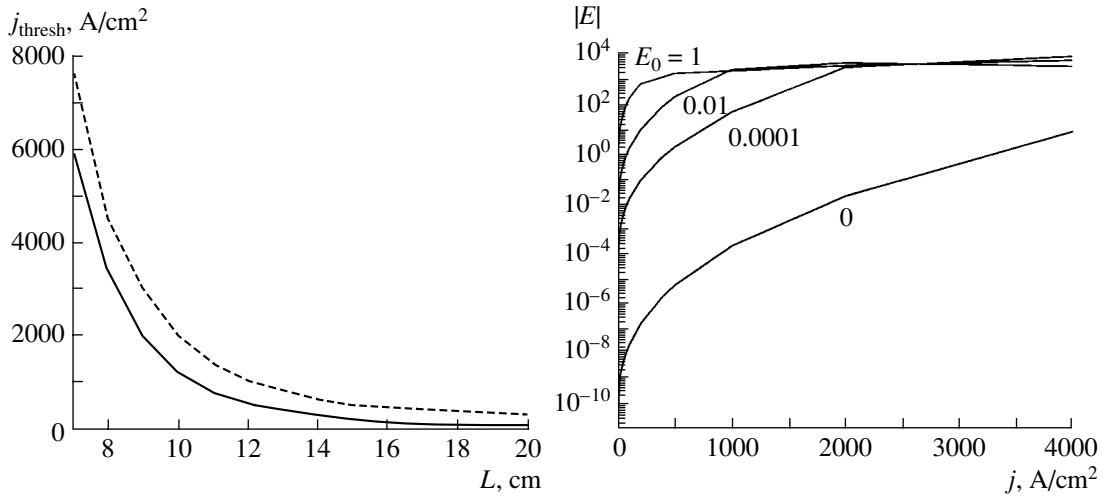

Fig. 5.

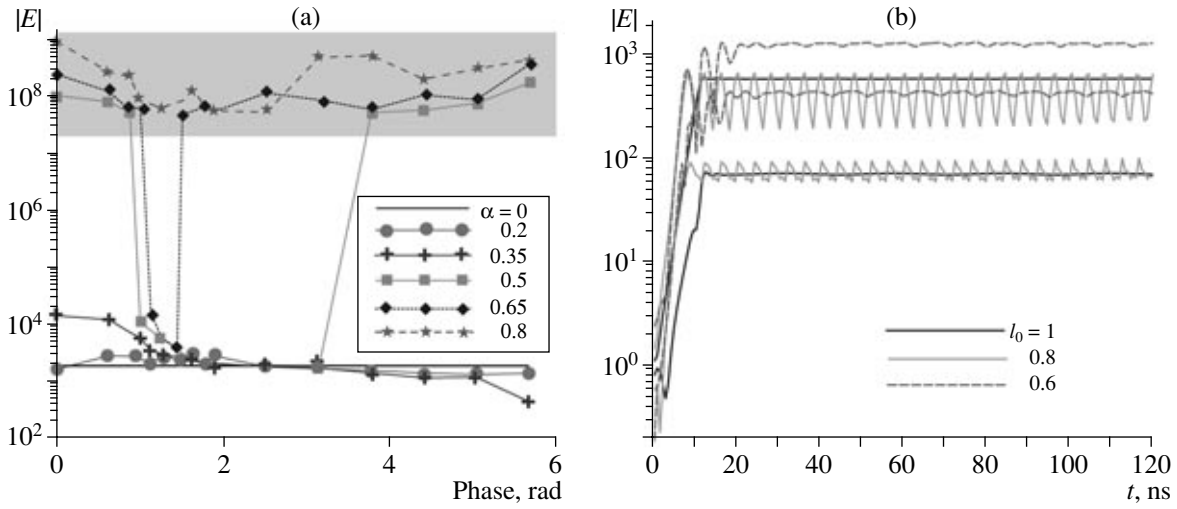

Fig. 6.

ceases to depend on the length. Our numerical computations have shown that the presence of an external wave ($E_0 \neq 0$) also reduces the generation threshold.

Laue geometry was also analyzed in the simulation (Fig. 2). Figure 5b shows the amplitude of the electromagnetic field as a function of the current density for various amplitudes of incident waves ($\chi_0 = 0.1$, $L = 80$). The curve with the amplitude $E_0 = 0$ corresponds to the SASE regime. The other curves demonstrate the regime of amplification. For the parameters chosen, self-amplified stimulated emission occurs at large current densities. As the interaction length increases, the current density required for this regime reduces.

Now, let us analyze the results obtained for VFEL simulation with external mirrors (the geometry shown in Fig. 2b). The presence of external mirrors reduces the generation threshold, thus, making it possible to achieve the regime of stationary saturation at lower currents. We present the numerical results for the case of an incident wave with the amplitude $E_0 = 0.1$ for several values of the reflection coefficient $\alpha_1 = \alpha$ (the other coefficients in (7) are assume to vanish: $\alpha_i = 0$, $i = 2, 3, 4$). The variant $\alpha = 0$ corresponds to the case of absence of mirrors. Figure 6a shows the wave amplitude as a function of the phase φ_1 varying from 0 to 2π. As the reflection coefficient becomes higher than $\alpha = 0.5$, there appear two distinct domains: with stable and unstable solutions. The domain with an unstable blowing-up solution is shown by the shaded area in Fig. 6a. The presence of such a domain can be explained by the fact that the phases of the generated wave depend on the phases of the reflection from the Bragg mirrors. Changing α, we thus change the synchronism

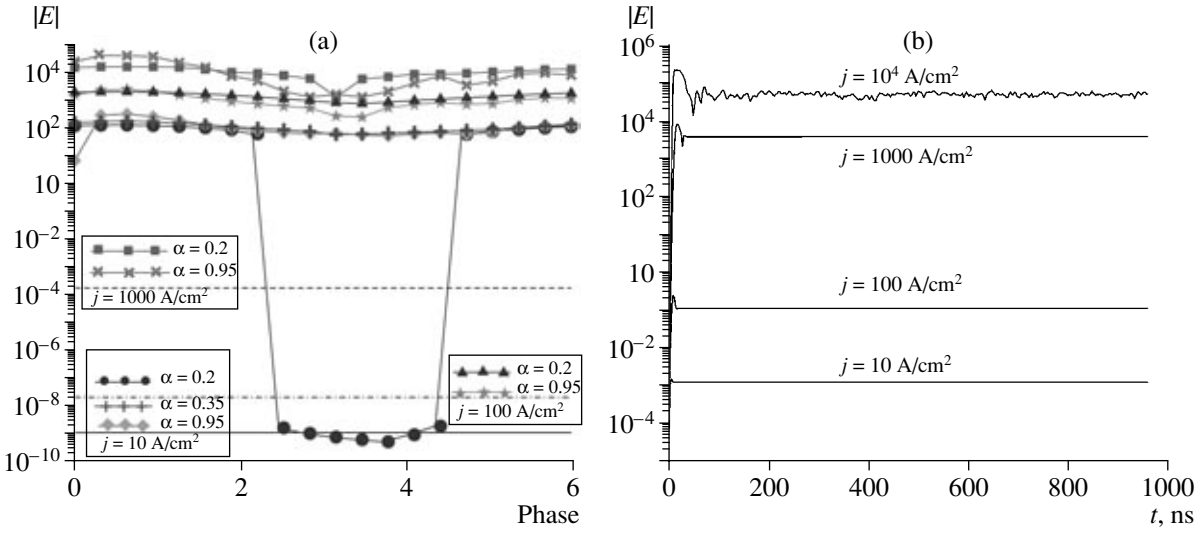

Fig. 7.

conditions between the electron beam and the wave. When synchronism between the electrons and the wave is violated, the current term becomes small and the system of equations becomes linear. It is well known that a homogeneous linear system of equations has either the trivial solution or an infinite number of solutions (when its determinant is zero). This uncertainty may lead to blowup in numerical modeling. This case corresponds to the shaded area shown in Fig. 6a. The simulation of the amplification regime in Laue geometry with external mirrors is presented in Fig. 7a. The numerical results shown correspond to the beam current densities $j = 10$ A/cm^2 (no mirrors, the solid curve), $j = 100$ A/cm^2 (no mirrors, the dash-and-dot curve), and $j = 1000$ A/cm^2 (no mirrors, the dashed curve) for various α. The generator in Laue geometry operates at current densities that are several orders of magnitude lower than the laser in the SASE regime (for the same length of the interaction region).

Finally, we discuss the results of the simulation obtained for nonstationary system (4). The results of the simulation obtained for the stationary case should be repeated for the nonstationary case, and this has been done. Additionally, various plots showing bifurcations of the solutions were obtained. In particular, Fig. 6b shows the amplitudes of the incident and diffracted waves at the target exit for various Bragg geometry parameters l_2. A variation in only one parameter changes the qualitative behavior of the solution. We see curves with a precisely repeating oscillation period, several oscillations imposed on a single curve, and a steady state solution. As the parameters of the system vary, one regime of generation switches to another according to the transition of the parameters of order from one critical value to another. A parameter of order can be defined as the electron beam density, the asymmetry factor, the absorption coefficient, frequency, etc. Figure 7b shows the results of the simulation obtained for a nonstationary system in Laue geometry. Here, bifurcations were found to occur at the very high beam current density $j = 10^4$ A/cm^2.

6. CONCLUSIONS

Thus, our numerical experiments confirmed that the mathematical models proposed and the numerical algorithms developed can effectively be applied to the simulation of nonlinear regimes in VFEL operation. The numerical results agree with analytical estimates obtained in the linear approximation. The analysis performed suggests that VFEL operation can be numerically modeled in planned experiments. The results obtained allow us to determine the possible types of electron-beam instabilities and generation regimes in VDFB geometry and their dependence on various parameters.

ACKNOWLEDGMENTS

The authors thank V.G. Baryshevsky for his encouragement and interest in this work.

REFERENCES

1. S. Andruszkow, "First Observation of Self-Amplified Spontaneous Emission in a Free Electron Laser at 109 nm Wavelength," Phys. Rev. Lett. **85**, 3825–3829 (2000).
2. Y. C. Huang, C. S. Hsue, R. H. Pantell, and T. I. Smith, "The FEL and IFEL Design Study for the Proposal NTHU Photon-Electron Dynamics Laboratory," Nucl. Instr. Methods Phys. Res. A **429**, 430–434 (1999).
3. A. V. Elzhov, N. S. Ginzburg, A. K. Kaminsky, *et al.*, "Features of FEM for Testing of High-Gradient Accelerating Structures of Linear Colliders," *Proceedings of Eighth European Particle Accelerator Conference (EPAC'2002), Paris, 2002*, pp. 2308–2310.
4. M. Korfer, "The TTF-FEL Status and Its Future As X-Ray User Facility," Nucl. Instr. Methods Phys. Res. A **483**, 34–39 (2002).
5. V. G. Baryshevsky and I. D. Feranchuk, "Parametric Beam Instability of Relativistic Charged Particles in a Crystal," Phys. Lett. A. **102**, 141–144 (1984).
6. V. G. Baryshevsky and I. D. Feranchuk, "Quantum Theory of Parametric X-Ray Generator with Allowance for Multiwave Diffraction," Vesti Akad. Nauk Belarusi, Ser. Fiz.-Mat. Nauk, No. 2, 79–86 (1985).
7. V. G. Baryshevsky, K. G. Batrakov, A. Gurinovich, *et al.*, "First Lasing of a Volume FEL (VFEL) at a Wavelength Range 4–6 mm," Nucl. Instr. Methods Phys. Res. A **483**, 21–23 (2002).
8. V. G. Baryshevsky, I. Ya. Dubovskaya, and I. D. Feranchuk, "Cherenkov Beam Instability of Charged Particles in a Three-Dimensional Spatially Periodic Medium," Vesti Akad. Nauk Belarusi, Ser. Fiz.–Mat. Nauk, No. 1, 92–97 (1988).
9. K. G. Batrakov and I. Ya. Dubovskaya, "Cherenkov Beam Instability in a Spatially Periodic Medium," Vesti Akad. Nauk Belarusi, Ser. Fiz.–Mat. Nauk, No. 5, 82–89 (1990).
10. V. G. Baryshevksy, K. G. Batrakov, and I. Ya. Dubovskaya, "Parametric (Quasi-Cherenkov) X-Ray Free Electron Laser," J. Phys. D: Appl. Phys. **24**, 1250–1257 (1991).
11. V. G. Baryshevsky, K. G. Batrakov, and I. Ya. Dubovskaya, "Parametric (Quasi-Cherenkov) FEL," Vesti Akad. Nauk Belarusi, Ser. Fiz.–Mat. Nauk, No. 1, 53–60 (1991).
12. V. G. Baryshevsky, K. G. Batrakov, and I. Ya. Dubovskaya, "Optical Parametric Free Electron Laser with Three-Dimensional Distributed Feedback," Vesti Akad. Nauk Belarusi, Ser. Fiz.–Mat. Nauk, No. 3, 99–106 (1992).
13. V. G. Baryshevsky, K. G. Batrakov, and I. Ya. Dubovskaya, "Induced Radiation from a Relativistic Electron Beam in Periodic Structures," Phys. Stat. Sol. B **169**, 235–243 (1992).
14. V. G. Baryshevsky, K. G. Batrakov, and I. Ya. Dubovskaya, "Surface Quasi-Cherenkov Free Electron Laser," Nucl. Instrum. Methods Phys. Res. A **341**, 274–276 (1994).
15. V. G. Baryshevsky, K. G. Batrakov, I. Ya. Dubovskaya, and S. N. Sytova, "Visible Surface Quasi-Cherenkov FEL," Nucl. Instrum. Methods Phys. Res. A **358**, 508–511 (1995).
16. V. G. Baryshevsky, K. G. Batrakov, and I. Ya. Dubovskaya, "Formation of Distributed Feedback in an FEL under Multiwave Diffraction," Nucl Instr. Methods Phys. Res A **358**, 493–496 (1995).
17. V. G. Baryshevsky, K. G. Batrakov, and I. Ya. Dubovskaya, "Parametric X-Ray FEL Operating with External Bragg Reflectors," Nucl. Instrum. Methods Phys. Res. A **375**, 292–294 (1996).
18. V. G. Baryshevsky, K. G. Batrakov, and I. Ya. Dubovskaya, "Volume Quasi-Cehernkov FEL in mm-Spectral Range," *Free Electron Lasers* (Elsevier Sci. II-75, 1996/1997).
19. V. G. Baryshevsky, K. G. Batrakov, and V. I. Stolyarsky, "Application of Volume Diffraction Grating for Terahertz Lasing in Volume FEL (VFEL)," Nucl. Instrum. Methods Phys. Res. A **507**, 93–96 (2003).
20. V. G. Baryshevsky, "Volume Free Electron Lasers," Nucl. Instrum. Methods Phys. Res. A **445**, 281–283 (2000).
21. V. G. Baryshevsky and K. G. Batrakov, "Dependence of Volume FEL (VFEL) Threshold Conditions on Undulator Parameters," Nucl. Instrum. Methods Phys. Res. A **483**, 531–533 (2002).
22. N. S. Ginzburg, N. Yu. Peskov, and A. S. Sergeev, "Dynamics of Free Electron Lasers with Two-Dimensional Distributed Feedback," Optics Commun. **112**, 151–156 (1994).
23. N. Ginzburg, R. Rosental, N. Peskov, *et al.*, "Modeling of a Planar FEL Amplifier with a Sheet Relativistic Electron Beam," Nucl. Instrum. Methods Phys. Res. A **483**, 255–258 (2002).
24. N. S. Ginzburg, S. P. Kuznetsov, and T. N. Fedoseeva, "Theory of Transients in a Relativistic Backward Wave Tube," Izv. Vyssh. Uchebn. Zaved., Radiofiz. **21**, 1037–1052 (1978).
25. N. S. Ginzburg, R. M. Rozental', and A. S. Sergeev, "On the Synthesis of Radiation Spectrum in a Sectioned Relativistic Backward Wave Tube," Pis'ma Zh. Tekh. Fiz. **29** (4), 71–80 (2003) [Tech. Phys. Lett. **29**, 164–167 (2003)].
26. V. N. Abrashin, A. O. Grubich, and S. N. Sytova, "Nonlinear Stage in Development of Relativistic Electron Beam Cherenkov Instability," Mat. Model. **3** (8), 21–29 (1991).
27. S. N. Sytova, "A Numerical Method for Solving One Problem in Nuclear Physics," Vesti Akad. Nauk Belarusi, Ser. Fiz.–Mat. Nauk, No. 2, 44–50 (1993).
28. S. N. Sytova, "A Numerical Method for Solving Hyperbolic Systems with Singularities," Differ. Uravn. **32**, 986–989 (1996).

29. S. N. Sytova, Candidate's Dissertation in Mathematics and Physics (Belarus. Gos. Univ., Minsk, 1997).
30. V. G. Baryshevsky, K. G. Batrakov, I. Ya. Dubovskaya, and S. N. Sytova, "The Nonlinear Analysis of Visible Quasi-Cherenkov FEL," in *Abstract of 21st International Free Electron Laser Conference (FEL99)* (Hamburg, Germany, 1999).
31. S. Sytova, "On Numerical Methods for Modeling of Terahertz Sources Based on Low Energy Relativistic Beams," *Proceedings 3rh International Conference EFS2000* (IMI, 2000, Vilnius), pp. 237–244.
32. S. N. Sytova, "Numerical Methods in Modeling of Volume Free Electron Lasers," in *Fundamental and Applied Physics Research over 1986–2001* (BGU, Minsk, 2001), pp. 212–226 [in Russian].
33. S. N. Sytova, "Finite Difference Methods in Problems Modeling Volume Free Electron Lasers," Differ. Uravn. **37**, 976–981 (2001) [Differ. Equations **37**, 1067–1069 (2001)].
34. S. Sytova, "On Numerical Methods for One Problem of Mixed Type," Math. Model. Anal. **6**, 321–326 (2001).
35. S. N. Sytova, "Finite-Difference Methods for Generalized Transport Equations," Differ. Uravn. **38**, 999–1000 (2002) [Differ. Equations **38**, 1067–1069 (2002)].
36. K. Batrakov and S. Sytova, "Modeling of Quasi-Cherenkov Electron Beam Instability in Periodical Structures," Math. Model. Anal.**9** (1), 1–8 (2004).
37. S. L. Chang, *Multiple Diffraction of X Rays in Crystals* (Springer-Verlag, Berlin, 1984; Mir, Moscow, 1987).
38. K. Kim, "Three-Dimensional Analysis of Coherent Amplification and Self-Amplified Spontaneous Emission in Free Electron Lasers," Phys. Rev. Lett. **57**, 1871–1874 (1986).
39. A. A. Samarskii, *The Theory of Difference Schemes* (Nauka, Moscow, 1989; Marcel Dekker, New York, 2001).